FOSSIL ENERGY

NIPER-441
(DE90000212)

THE EFFECTS OF ROCK CHARACTERISTICS ON RELATIVE PERMEABILITY

Topical Report

By
D.R. Maloney
M.M. Honarpour
A.D. Brinkmeyer

January 1990

Performed Under Cooperative Agreement No. FC22-83FE60149

IIT Research Institute
National Institute for Petroleum and Energy Research
Bartlesville, Oklahoma

Bartlesville Project Office
U. S. DEPARTMENT OF ENERGY
Bartlesville, Oklahoma

This report has been reproduced directly from the best available copy.

Available to DOE and DOE contractors from the Office Of Scientific and Technical Information, P.O. Box 62, Oak Ridge, TN 37831; prices available from (615)576-8401, FTS 626-8401.

Available to the public from the National Technical Information Service, U.S. Department of Commerce, 5285 Port Royal Rd., Springfield, VA 22161

Price: Printed A03
Microfiche A01

NIPER-441
Distribution Category UC-122

THE EFFECTS OF ROCK CHARACTERISTICS ON RELATIVE PERMEABILITY

Topical Report

By
D.R. Maloney
M.M. Honarpour
A.D. Brinkmeyer

January 1990

Work Performed Under Cooperative Agreement No. FC22-83FE60149

Prepared for
U.S. Department of Energy
Assistant Secretary for Fossil Energy

Edith Allison, Project Manager
Bartlesville Project Office
P.O. Box 1398
Bartlesville, OK 74005

Prepared by
IIT Research Institute
National Institute for Petroleum and Energy Research
Box 2128
Bartlesville, OK 74005

TABLE OF CONTENTS

	Page
Abstract	1
Introduction	2
Experimental Procedures and Measurements	2
Selection And Preparation of Sandstone Samples	2
Measurements for Rock Characterization	3
Petrophysical Characterization and Calibration	4
Experimental Results	6
Rock Characteristics	6
Flow Characteristics	9
Discussion	11
Conclusions	12
Acknowledgments	13
References	13
Appendix A - X-ray, Microwave and Pressure Measurement System Improvements	24
Microwave System	24
X-ray Data Utilization and Calibrations	25
Pressure Measurement Systems	26
Appendix B - Automation of The Liquid Injection System	27

TABLES

1. Flow ratios during two- and three-phase relative permeability tests	14
2. X-ray diffraction analysis for unfired and fired cores	15
3. Fired Berea and Bentheimer rock characteristics	16

ILLUSTRATIONS

1A. XRD analysis of Berea sandstone before and after firing at 1,000° C	17
1B. XRD analysis of Bentheimer sandstone before and after firing at 1,000° C	17
2A. Grain diameter distributions by visual microscopic inspection	18
2B. Grain diameter distributions by image analysis	18
3A. Pore body diameter by visual microscopic inspection	19
3B. Pore body diameter by image analysis	19
4A. Mercury injection capillary pressure curves for Berea sandstone	20
4B. Mercury injection capillary pressure curves for Bentheimer sandstone	20
5. pH of effluent brine measured during water permeability measurement test on fired Berea	21
6. Ratio of gas to water relative permeability plot for Berea and Bentheimer rock samples	21
7. Imbibition and drainage oil/water relative permeabilities for Berea sandstone	22
8. Imbibition and drainage oil/water relative permeabilities for Bentheimer sandstone	22
9. Three-phase relative permeability results for Berea and Bentheimer sandstones	23
B-1. Schematic of pumping system for continuous injection of two liquid phases for relative permeability tests	32
B-2. Computer-pumps communication system	32
B-3. Detailed diagram of single pneumatic valve automation	32

THE EFFECTS OF ROCK CHARACTERISTICS ON RELATIVE PERMEABILITY

by D. R. Maloney, M. M. Honarpour, and A. D. Brinkmeyer

ABSTRACT

The goal of the work was to characterize two sandstone samples to the extent that differences in relative permeabilities could be attributed to differences in petrophysical or rock/fluid characteristics. Berea and Bentheimer sandstones were selected as the samples for this study because of their similar absolute permeabilities but slightly different petrographical properties.

The samples were tested extensively to evaluate petrographic, rock/fluid, and permeability characteristics. Petrographic analyses included X-ray diffraction (XRD); cation exchange capacity (CEC); and microscopic evaluation by scanning electron microscope (SEM), visual and computer- assisted image analysis. Rock/fluid tests included mercury injection capillary pressure, centrifuge capillary pressure and wettability, Amott tests, and resistivity tests. Permeabilities evaluated included absolute permeabilities measured with gas and with brine; two-phase gas-water, oil-water, and gas-oil relative permeabilities; and three-phase gas-oil-water relative permeabilities.

Results showed that petrographic properties of the two rocks were very similar. The primary differences between the two sandstones were that the Berea had larger amounts of microporosity and megaporosity than the Bentheimer sandstone. This determination was confirmed by SEM photographs and capillary pressure measurements. Differences in fluid flow characteristics were evident for the two samples when both two- and three-phase relative permeability results were compared. These differences include oil and brine residual saturations, hysteresis envelopes, mobile-phase saturations, and oil and water relative permeabilities. These are attributed to slight variations in pore size distributions and pore geometries.

INTRODUCTION

Relative permeability data are essential for almost all calculations of fluid flow in hydrocarbon reservoirs. The data are used in making engineering estimates of productivity, injectivity, and ultimate recovery from reservoirs for evaluation and planning of production operations and can be used to diagnose formation damage expected under various operational conditions. Relative permeability data are unquestionably one of the most important data sets in reservoir simulation studies. Relative permeability has a first-order dependency on saturation level. However, it is also influenced by wettability, pore geometry, temperature, and capillary forces. Few studies have been conducted to investigate the effect of pore geometry on relative permeability because multiphase relative permeability data are experimentally difficult to obtain, and few experimental programs have been undertaken in the systematic manner required to provide sufficient data to evaluate and differentiate the effect of pore geometry from that of wettability. Additionally, obtaining two similar natural sandstone samples having identical petrophysical, petrographical, and wettability properties but dissimilar pore characteristics is extremely difficult.

The objective of this research was to characterize two samples to the extent that differences in relative permeability results could be associated with differences in pore or rock/fluid characteristics. This work was concentrated in two areas: examination of petrophysical, petrographical, and rock/fluid properties; and examination of their interrelationships with relative permeabilities.

EXPERIMENTAL PROCEDURES AND MEASUREMENTS

Selection And Preparation of Sandstone Samples

Two sandstone samples were selected for evaluation. High-permeability sandstone rock samples were chosen to minimize the effects of capillarity on relative permeability results. Several rock types were evaluated and discarded because of layering or inconsistent horizontal and vertical permeabilities. Berea and Bentheimer sandstones were finally selected for this investigation. Berea sandstone has been used extensively for petroleum research, and its general characteristics are well known. Bentheimer sandstone, a rock from a German quarry, was selected as the second sandstone type because of its high permeability and homogeneity. All of the Berea samples were cut from a single block of rock. Similarly, all Bentheimer samples were cut from a single block of the sandstone. Both fired and unfired samples of the two sandstones were prepared. The firing was performed at 1,000° C to oxidize organic materials and desensitize indigenous clays to minimize any changes in flow characteristics of the rocks during relative permeability measurements.

Measurements for Rock Characterization

Unfired and fired samples were analyzed using X-ray diffraction (XRD) and wet chemistry techniques to distinguish differences in mineralogy between the two samples and to evaluate the effect of firing on the clay minerals. Cation-exchange-capacity (CEC) tests were conducted to quantify the potential of each sample for cation absorption. CEC tests were conducted using the ammonium acetate technique.

Thin sections were cut from fired and unfired pieces of the two sandstones. Petrographic analyses performed on the thin sections included: inspecting magnified images of the rocks using a scanning electron microscope (SEM); visual microscopic examinations; and computer-aided microscopic image analyses. SEM evaluations were conducted using an ISI Super IIIA microscope with 100x and 300x magnifications. Visual microscopic evaluations were conducted using a Zeiss petrographic microscope with a calibrated micrometer eyepiece and 100x magnification. The limit of resolution for visual microscopic measurements and counts was in the 1 to 10 μm range. Pores or grains smaller than 1 μm were not included in counts. Computer-aided image analyses were conducted using a microcomputer-based image analysis system. The system consists of a Dage MTI camera mounted on a Nikon light microscope. The output from the camera is interfaced with the microcomputer. The microcomputer digitizes the images and performs various petrographic measurements and calculations using software by American Innovision. For this project, the resolution of the measurements taken by computer-aided image analysis was about 7 - 10 μm due to the screen resolution of 1.5 μm/pixel. Features with dimensions less than 7 - 10 μm were ignored in grain and pore size number distribution calculations.

Pore and pore-throat sizes were also evaluated using mercury injection capillary pressure techniques. Using this well known technique, the volume of mercury injected into a core plug and the coincident increase in pore pressure is used to describe the saturation and pore/throat size distribution.

Centrifuge techniques were used to determine capillary pressures as functions of water and oil saturations and to quantify wettability indexes. The centrifuge used for these experiments was a Beckmann J6M machine that was modified by adding special centrifuge buckets, a bottom-mounted strobe assembly, and a top-mounted video camera. The strobe flashes each time the sample is exactly positioned under the viewing window. The video camera sends an image of the selected centrifuge tube to a video monitor, which allows monitoring and measurement of liquid volumes in the calibrated centrifuge tubes. Centrifuge tests were conducted on 3.8 cm diameter by 3.8 cm long plugs at rotational speeds from 400 to 4,000 RPM. The 4,000 RPM speed provided more than 30 psi of capillary pressure in the oil-water system. Sufficient time was allowed for measurements to stabilize at each of 10 data points

per cycle (drainage and imbibition).

Amott tests were also conducted on 3.8 cm diameter by 3.8 cm long plugs of fired Berea and Bentheimer sandstones. The plugs were initially saturated with brine (1% NaCl). Next, the plugs were centrifuged in oil (Soltrol 100 tagged with 10% by volume iodododecane) to reduce brine saturations to residual levels. The plugs were placed in imbibition cells in brine for 1 week. The volume of brine imbibed into each plug was measured from the volume of oil expelled from the plugs. Oil imbibition was measured in a similar manner. The plugs were centrifuged in brine to reduce oil saturations to irreducible levels. The plugs were then placed in imbibition cells filled with oil for 1 week, and the amount of oil imbibed by each plug was recorded.

Petrophysical Characterization and Calibration

An experiment was conducted on a Berea sandstone core plug to evaluate the variation in permeability with length. The purpose of this experiment was to evaluate the effect of pressure port placement on average petrophysical properties of the core. The dry plug was installed in a coreholder that had multiple pressure taps at intermediate locations along the length of the coreholder sleeve. A four-way electomechanical valve was installed in a manner which allowed a single differential pressure transmitter to be used to measure pressure drops between the outlet, inlet, and 3 intermediate pressure taps along the length of the plug. A single transmitter was used to eliminate errors in comparing output from different pressure measurement devices. Permeabilities were calculated from Klinkenberg-corrected gas permeability data. After completing the test, the plug orientation was reversed and a similar test was performed.

Porosities for both the Berea and Bentheimer sandstones were determined on 2.5 cm diameter by 2.5 cm long samples using a Boyle's law gas expansion technique. Electrical resistivities were measured using 3.8-cm sandstone plugs under two-phase flow conditions using nitrogen gas and 1% NaCl brine (1% by weight salt in deionized water) as the permeating fluids.

Samples of the sandstones used for relative permeability experiments were 15 cm in length with rectangular cross sections of 2.5 cm by 5.1 cm. The samples and their Lucite end-pieces were jacketed with a thin layer of epoxy resin followed by a 0.8-cm-thick jacket of Castolite-AP clear casting plastic. Pressure ports were drilled and tapped in the casting plastic to provide pressure taps along the length of each sample. The pressure taps were spaced 5 cm apart.

Gas permeabilities and dry microwave and X-ray scan data were established for the dry cores, then the cores were saturated with 1% NaCl brine (water and brine are used synonymously for brine in this

report). Water permeabilities were calculated from measurements taken during waterflood tests. Additionally, the pH of the water effluent from each core was measured. After establishing the absolute permeability to brine for each of the samples and obtaining X-ray and microwave scan data, gas/water calibrations were developed using the microwave and X-ray data. Gas-water relative permeability experiments were then conducted.

Next, each core was cleaned by flushing first with about 10 pore volumes (PV) of isopropyl alcohol followed by 10 PV of pentane and sufficient nitrogen gas to evaporate the pentane. Microwave and X-ray scans and gas permeabilities of the dry rock were used to confirm that each sample was indeed clean and dry. After resaturating the samples with water, water-oil relative permeability tests were conducted. The oil used in these tests was Soltrol 100 tagged with 10% by volume iodododecane. The viscosity of the oil was 1.2 cP at the test conditions. The iodododecane tag was added to provide a better contrast between the oil and water response for X-ray calibrations. Calibrations were developed to relate X-ray and microwave scan results with oil and water saturation conditions. Thereafter, gas-oil relative permeability tests were conducted. Attempts were made to conduct the gas-oil relative permeability tests with residual water saturation present in the cores.

X-ray and microwave calibrations were then developed for each core for a three-phase pore fluid system consisting of gas, water, and oil. Each core was cleaned and saturated with water. Prior to initiating the three-phase tests, the cores were flooded with oil and gas, then flooded with water only to establish residual oil and gas saturations. Three-phase relative permeability tests were then conducted.

All of the flow experiments were conducted at 23° C with no backpressure. The Bentheimer sample was tested unconfined. The Berea sample was tested in the microwave coreholder with a confining pressure of 11 atm. Fluctuations in the confining pressure applied to the Berea sample occurred as a result of temperature changes in the laboratory. Initially, the confining pressure was adjusted to maintain the 11-atm level. This was found to be a mistake as changes in the volume of silicone oil in the coreholder caused subsequent changes in the baseline X-ray attenuation for the system which could not be filtered from the X-ray data. Variations in temperature also caused changes in the viscosities of the test fluids. After these effects were noted, steps were taken to eliminate sources of error from thermal effects. The temperature control system for the laboratory was redesigned to reduce temperature deviations from the set point. The temperature in the laboratory was stabilized to within 2° C of the set point.

Because of the high absolute permeabilities for these sandstones, injection pressures were about 1.2 atm (abs) during two-phase flow experiments and lower than 3 atm (abs) for three-phase experiments.

Pressure drops across 5 cm lengths of the sandstones were less than 0.7 atm in all flow tests. Table 1 lists the flow rate ratios used during two-phase and three-phase relative permeability experiments. Liquid flow rates were limited to a maximum of 400 ml/hr which is the maximum output from the ISCO syringe pumps that were used. Other descriptions of test procedures and methods used in this project have been described previously.[1] Modifications and improvements to the relative permeability system implemented during the course of this investigation are described in appendices A and B.

EXPERIMENTAL RESULTS

Rock Characteristics

After firing, the clay mineral peaks in XRD measurements disappeared and indicated a collapse of their layered crystalline structure. Quartz and feldspar grains were not significantly altered by firing; however, iron sulfides, siderite, and ferroan dolomite were converted to hematite and gave the rock a reddish color. Bentheimer sandstone contained less clay than Berea before firing, but they showed extreme similarities in mineralogical characteristics after firing. Results of the XRD analysis of both cores before and after firing are presented in table 2 and figure 1. These similarities were further confirmed by CEC measurements using wet chemistry. Cation exchange capacities of both Berea and Bentheimer sandstone cores were close to 0.21 meq/100 g before firing and were reduced to zero when fired.

The petrographic characteristics of the two sandstone samples are given in table 3. Evaluation of SEM results for the two rocks at 300x magnification indicates that the Berea sandstone exhibits greater microporosity than the Bentheimer sandstone. In this context, microporosity is defined as pore features with dimensions in the submicron range.

Both visual microscopic and image analysis number distributions were determined for grains or pores greater in size than 10 μm. These examinations indicated that both Berea and Bentheimer sandstones have similar grain size distributions, with Bentheimer sandstone having a slightly wider range of grain size. Grain size distributions are shown in figures 2A and 2B. Compared to that of Berea sandstone, the Bentheimer grain size distribution was skewed toward larger grain sizes. Median grain sizes for Berea and Bentheimer sandstones were 180 and 190 μm, respectively, as indicated by computer-aided image analysis. Grain sizes determined by visual microscopic examination were higher than those obtained from computerized analyses by about 60 μm. The values obtained from computer analysis are considered more representative because they are operator-independent and are obtained from a larger population set.

Pore dimensional characteristics were also evaluated from visual microscopic, image analysis, and mercury injection capillary pressure measurements. The visual microscopic inspection yielded median pore body diameters of 80 μm for the Berea and 120 μm for the Bentheimer. Figures 3A and 3B show pore body diameter distribution results. The range of measurable pore body diameters was from 40 to 320 μm for each sample. The pore diameter distribution of Berea was slightly skewed toward smaller sizes compared to that of the Bentheimer. Computer-aided image analysis yielded similar results, with the Bentheimer having a larger number of medium sized pores (60 to 140 μm) and a lower number of pore diameters greater than 140 μm compared to the Berea. In this report, the porosity from pores with diameters greater than 140 μm is referred to as megaporosity. The image analysis technique showed a larger number of pores for each sample in the 40 to 80 μm (arbitrary cutoff) range compared with the distributions determined from visual microscopic examinations. The microscope used with the image analysis technique was more powerful than that used for the visual technique, which provided a higher degree of resolution and accuracy by the image analysis technique.

Mercury injection capillary pressure results indicated that approximately 80% of the pore throats within both Berea and Bentheimer samples were in the 1 to 60 μm range (see figs. 4A and 4B). The Berea sample had slightly larger pore throat diameters than the Bentheimer yielding lower capillary pressures at lower mercury saturations. However, the Berea also had slightly greater microporosity. At 50% mercury saturation, the average pore throat diameter for the Berea was 16 μm, whereas that of the Bentheimer was 10 μm.

The results from centrifuge capillary pressure tests performed on the Berea and Bentheimer samples were very different. At the end of the drainage test (water saturation decreasing) the water saturation for the Berea was 11.7% (percent of pore volume), whereas the value for the Bentheimer sample was 4.9% at an oil capillary pressure of 30 psi. For capillary pressures lower than 10 psi, Bentheimer showed higher oil trapping than the Berea in the imbibition cycle of the centrifuge capillary pressure test. At the end of the imbibition test, the oil saturations for both samples were 4.8% at a water capillary pressure of 30 psi. Both samples had wettability indexes close to 1 (Berea was 0.8 and Bentheimer was 1.0), which classifies the samples as strongly water-wet. These results show that oil trapping is similar for the two sandstones but is not simply a function of wettability. Since nonwetting phase trapping occurs in the larger pores, one can conclude from these tests that, at least for the larger pores, the pore size distributions for the two samples are very similar. This result is confirmed by the petrographic analyses.

Amott test results suggested that the Berea sandstone had more microporosity than the Bentheimer sandstone, and that neither of the two rock types was oil-wet. During the brine imbibition test, the Berea sandstone imbibed twice as much water as the Bentheimer sandstone. This may be attributed to the greater fraction of micropores in the Berea compared to the Bentheimer sandstone. Neither of the two sandstones imbibed any oil during the oil imbibition test, indicating that neither of the samples is preferentially oil-wet. These results were in confirmation of the centrifuge capillary pressure findings.

Flow Characteristics

A review of the results from the experiment to evaluate the effect of pressure port placement showed that end effects were present at both outlet and inlet core faces. Reversing the plug in the coreholder had no pronounced effect on permeability measurements. The lowest permeabilities were calculated for the inlet region of the plug, although some effect may have occurred due to pressure drops in the short length of tubing between the upstream pressure measurement location and the inlet face of the plug. The permeability in the center of the plug was identical regardless of plug orientation. The inlet permeability was approximately 64% of this value, whereas the permeability of the plug near the outlet was about 79% of this value. The equation

$$k_{ave} = L/\sum_{i=1}^{n} L_i/k_i \qquad (1)$$

where

k_{ave} = average permeability

L = plug length

L_i = length of section i

k_i = permeability of section i

n = number of sections

was accurate in representing the overall average permeability of the sample and was in excellent agreement with the overall permeability calculated from physical measurements. For this sample, the average permeability in the core is the harmonic average of the individual segments. These results show that the influence of end effects on rock permeability results may be minimized by measuring the pressure drop within the central portion of the rock sample.

Electrical resistivities of the Berea core sample were measured using both two- and four-electrode

techniques. The saturation exponent for the Berea core was found to equal 2 when the two-electrode method was used. This value is in good agreement with values suggested in the literature for clay-free sandstone core samples. The four-electrode method yielded higher resistivity than the two-electrode method at similar brine saturations. Bentheimer resistivity characteristics were not measured.

During the initial brine flow process after saturating the fired Berea sample, the pH of the effluent from the core sample was strongly basic (pH = 11). Figure 5 shows pH measurements recorded during the Berea brine permeability test as a function of pore volumes of brine injected. The pH values seemed to be independent of flow rates between 0.014 and 0.111 mL/sec but dependent of throughput and attributed to the dissolution of calcium oxide to form calcium hydroxide. The two spikes near 5.8 and 16.4 pore volumes coincide with periods during which the pump was shut down. Similar results for Berea have been reported by Shaw et al.[2] In a similar test, the pH of the effluent from the Bentheimer sample was close to neutral (6.5). In both cases, the pH of the injected brine was the same (6.5).

The absolute permeability of the Berea core was very similar to that of the Bentheimer core. Brine permeabilities were almost identical to air permeabilities. Permeabilities and porosities are listed in table 3.

Imbibition/drainage gas-brine relative permeability experiments are shown in figure 6 for the two samples as ratios of gas to brine relative permeabilities plotted against water saturation. The gas-water relative permeability ratios for the two samples were very similar except at very high water saturations. The data were normalized with respect to gas permeability measured at residual brine saturation. The water-gas relative permeability data from this investigation for the 2,050 md fired Berea sample was very similar to that of Oak et al.[3] measured on a 200-md fired Berea sandstone core. This may indicate that gas-water relative permeabilities for fired Berea cores are independent of permeabilities of the cores. The water relative permeability values were identical for both drainage and imbibition cycles. Three primary observations from the gas-water relative permeability data were: (1) Berea sandstone exhibits a higher residual water saturation and lower range of mobile saturation compared to Bentheimer; (2) the gas-brine relative permeability ratio of Bentheimer is higher than that of Berea at water saturations greater than 54%; whereas (3) at lower water saturations the two curves are very similar.

Imbibition/drainage oil-brine relative permeability tests were performed on both the Berea and Bentheimer samples. Results are shown in figures 7 and 8. A more pronounced hysteresis effect (difference between drainage and imbibition cycle trends) as well as higher residual brine saturation was noted for the Berea sample.

Three-phase relative permeability results for both Berea and Bentheimer sandstones are shown in figure 9. The data are normalized with respect to the two-phase oil permeability at residual oil saturation (1,227 md for Berea and 1,731 md for Bentheimer).

DISCUSSION

The water isoperms for the Berea sandstone were similar to those measured in previous experiments.[1] The water isoperms for both the Berea and Bentheimer samples were parallel to contours of equal water saturation, indicating that water relative permeabilities were functions of water saturations alone. The brine relative permeability of the Berea is lower than that of the Bentheimer at a given saturation condition. At high brine saturations, Bentheimer water relative permeabilities are twice as high as those of the Berea. At lower water saturations, the difference between the Berea and Bentheimer water relative permeabilities becomes much more significant (an order of magnitude). This is attributed to the presence of microporosity in Berea, causing restriction of water movement through the rock in the smaller pores. The envelope of water relative permeabilities in the three-phase system was much larger for the Bentheimer sample as compared to that for the Berea. The three-phase residual water saturation in Bentheimer was about 20% lower than that of the Berea.

The oil isoperms in the three-phase systems showed concavity toward the 100% oil saturation apex. The trends of the isoperms for both the Berea and Bentheimer sandstones were similar. The oil relative permeabilities of the two sandstone samples were similar at lower oil saturations, whereas the Berea sample showed much higher oil relative permeability at higher oil saturation. The Bentheimer sandstone exhibited a broader mobile saturation envelope than the Berea. At the low gas saturation, Bentheimer showed much more concavity than the Berea, indicating a stronger dependence of oil isoperms to gas saturation.

Gas isoperms for the Bentheimer sandstone showed little concavity toward the 100% gas saturation apex, while the Berea gas isoperms showed no apparent concavity. The three-phase gas relative permeabilities for the two samples were similar. The Bentheimer sandstone exhibited a larger mobile gas-saturation envelope.

When reviewed collectively, the results of this investigation indicate that one of the primary differences between the two sandstone samples is the degree of microporosity that each sample exhibits. Thin section evaluation by either visual microscopic or computer-aided image analysis techniques are not by themselves sufficient to evaluate microporosity due to limits in microscopic resolution.

The scanning electron microscope was an effective tool for showing microporosity because it

provides resolution in the submicron range. Mercury injection and centrifuge capillary pressure techniques, together with wettability results, were useful for identifying the presence of microporosity but insufficient for quantifying the degree of microporosity associated with each sample. A method for describing the microporosity of a sample quantitatively or by an index would provide another useful characteristic for comparison among samples.

The second major difference between the two sandstone samples is that the Bentheimer sample has a larger number of medium-sized pores (60 - 140 μm) and a lower number of pore diameters greater than 140 μm (megaporosity) compared to the Berea. This may be responsible for the fast decline in oil relative permeability isoperms when gas occupies the largest group of pores. Since the results of this investigation show that differences in relative permeabilities were directly attributable to differences in microporosity and megaporosity, the development of indices to characterize pore size distributions may be needed for determining correlations among relative permeabilities and other parameters.

CONCLUSIONS

The following observations and conclusions were made as a result of this steady-state experimental study performed on Berea and Bentheimer sandstones.

1. The two selected sandstone samples were similar in all petrophysical and petrographical properties and rock/fluid interaction properties but were different in pore throat/body extremities (microporosity and megaporosity).

2. Residual oil saturation during oil-water two-phase flow was lower for the Bentheimer than the Berea sandstone.

3. The mobile-phase saturation during the oil-water relative permeability test was larger for the Bentheimer sample as compared to the Berea sample.

4. The oil-water relative permeability results for both samples exhibited appreciable hysteresis effects.

5. For both samples, water relative permeabilities during three-phase flow were functions of water saturation alone. The Berea brine relative permeabilities were lower than those of the Bentheimer sample at each saturation condition. This result is attributed to the greater microporosity for the Berea compared to the Bentheimer sandstone.

6. The oil isoperms in the three-phase systems showed concavity toward the 100% oil apex, indicating that oil relative permeabilities are influenced by all three fluid saturations. At low gas saturation, Bentheimer shows more concavity than Berea, indicating a stronger dependence of oil isoperms to gas saturation. This result is attributed to the lower degree of megaporosity for the Bentheimer compared to the Berea sandstone.

7. Neither of the gas isoperms for the two samples showed much concavity toward the 100% gas apex, indicating that gas permeabilities are primarily a function of gas saturation.

8. The Bentheimer sample exhibited a larger mobile saturation envelope compared to the Berea sandstone.

9. As both micro- and mega-porosity appear to have a significant influence on relative permeability characteristics, a sorting index describing pore size characteristics is needed for classifying rock types and for use in developing relative permeability correlations.

ACKNOWLEDGMENTS

This work was performed for the U. S. Department of Energy under Cooperative Agreement DE-FC22-83FE60149. The authors acknowledge Herbert B. Carroll, Jr., Min K. Tham, Aaron Cheng, Mike Madden, and Bill Linville of NIPER for their support and help throughout the duration of this project. We appreciate the support of the U.S. Department of Energy for financing this research project, and Edith Allison, DOE Project Manager. The authors also thank Willis Waldorf for his assistance in the lab for relative permeability experiments, Shogo Suzuki, JAPEX for conducting the centrifuge capillary pressure experiments, and Edna Hatcher for typing this manuscript.

REFERENCES

1. Maloney, D., S. Mahmood, and M. Honarpour. The Effects of Viscous Forces on Three-Phase Relative Permeability. Department of Energy Report NIPER 392. NTIS order No. DE89000737.

2. Shaw, J., P. Churcher, and B. Hawkins. The Effects of Firing on Berea Sandstone. Pres. at the SPE Int. Symp. on Oilfield Chemistry, Houston, TX, Feb. 8-10, 1989. SPE paper 18463.

3. Oak, M., L. Baker, and D. Thomas. Three-Phase Relative Permeability of Berea Sandstone. Pres. at the SPE/DOE Enhanced Oil Recovery, Tulsa, OK, Apr. 17-20, 1988. SPE/DOE paper 17370.

TABLE 1. - Volumetric flow ratios during two- and three-phase relative permeability tests

Test	Condition	Gas	Water	Oil
Two-phase				
Gas-Water	brine perm	0	1	0
	drainage cycle	20	1	0
		250	1	0
	"	1000	1	0
	"	8000	1	0
	residual water	1	0	0
	imbibition cycle repeats in reverse direction			
Oil-Water	water perm	0	1	0
	drainage cycle	0	80	1
	"	0	15	1
	"	0	2	1
	"	0	0.25	1
	"	0	0.025	1
	residual water	0	0	1
	imbibition cycle repeats in reverse direction			
Gas-Oil with IResidual Water Sat.	oil perm.	0	0	1
	oil draining	20	0	1
	"	250	0	2
	"	1000	0	1
	"	8000	0	1
	residual oil	1	0	0
	imbibition cycle repeats in reverse direction			
Three-phase	gas-water, oil	150	4.5	1
		12000	4.5	1
		12000	12.5	1
		12000	1.25	1
	residual gas, oil	0	1	0
	water-oil, gas	1	0.7	0.007
		1	0.3	0.02
		1	0.02	0.3
		1	0.007	0.7
	residual water, gas	0	0	1
	gas-oil, water	60	1	20
		4800	1	20
		4800	1	5
		4800	1	1
		4800	1	0.04
	residual water, oil	1	0	0

TABLE 2. - X-ray diffraction analysis for unfired and fired cores

Mineral	Unfired Berea, %	Fired Berea, %	Unfired Bentheimer, %	Fired Bentheimer, %
Quartz	94	98	97.5	98
Feldspar	3	2	2	2
Calcite	T	T	T	T
Dolomite	1	T	T	T
Siderite	T	T	T	T
Kaolinite	2	-	0.5	-
Cholorite	T	-	-	-
Illite/Mica	T	-	-	-
Hematite	-	T	-	T

T = Trace amount.

TABLE 3. - Fired Berea and Bentheimer rock characteristics

Characteristic	Berea	Bentheimer
Porosity, %	26.1	24.7
Absolute permeability, md	2,050	2,388
Grain density, g/cm^3	2.670	2.665
Grain size distribution	normal	wide range, skewed toward larger grain sizes.
Median grain size, μm	180	190
Pore body distribution	skewed toward smaller sizes	normal
Median pore body dia., μm	80	120
Range of pore body dia., μm	40 - 320	larger number of 60 - 140 μm pores, lower number of pores greater than 140 μm.
Pore throat distribution	wider distribution greater microporosity	narrower distribution lower microporosity.
Pore throat dia. at 50% mercury saturation, μm	16	10
Effluent pH during flow[1]	11	6.5
Amott test		
water imbibed, % PV	61.4	30.1
oil imbibed, % PV	0	0
Centrifuge irr. water sat., % PV	11.7	4.9
Centrifuge irr. oil sat., % PV	4.8	4.8

[1]pH of the injected brine was 6.5.

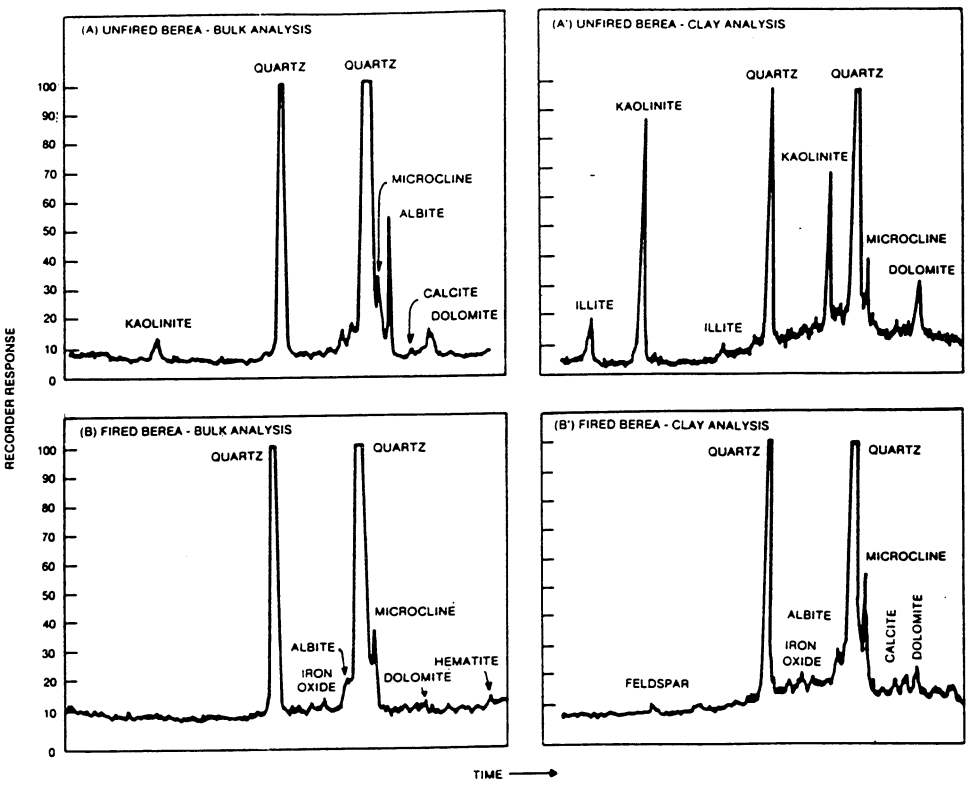

FIGURE 1A. - XRD Analysis of Berea sandstone before and after firing at 1,000° C.

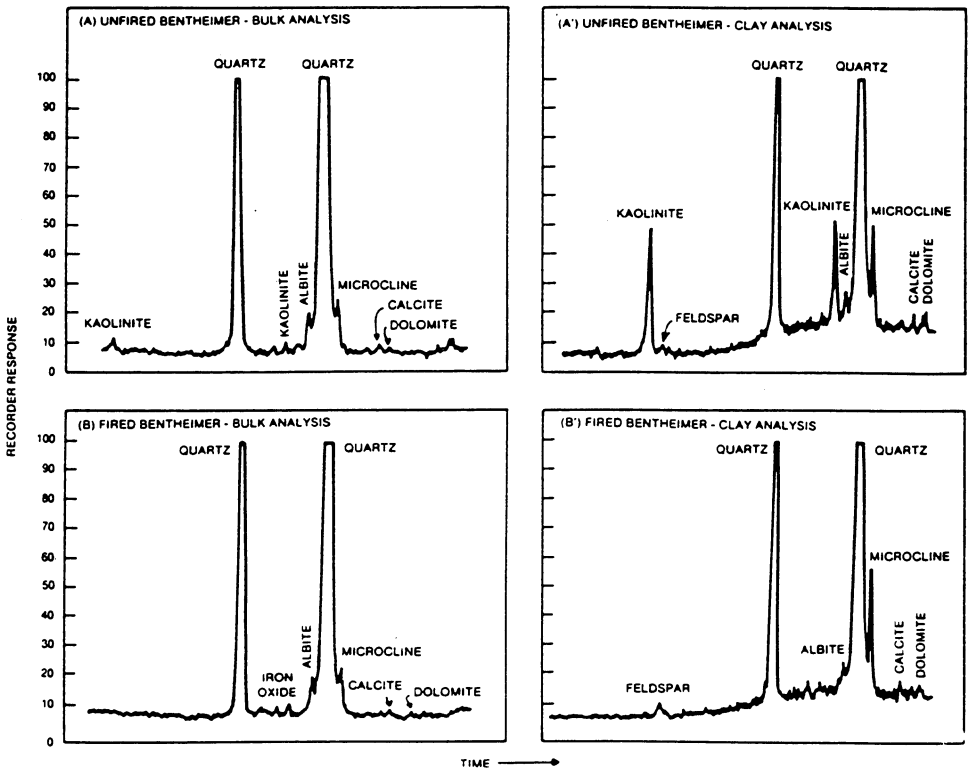

FIGURE 1B. - XRD Analysis of Bentheimer sandstone before and after firing at 1,000° C.

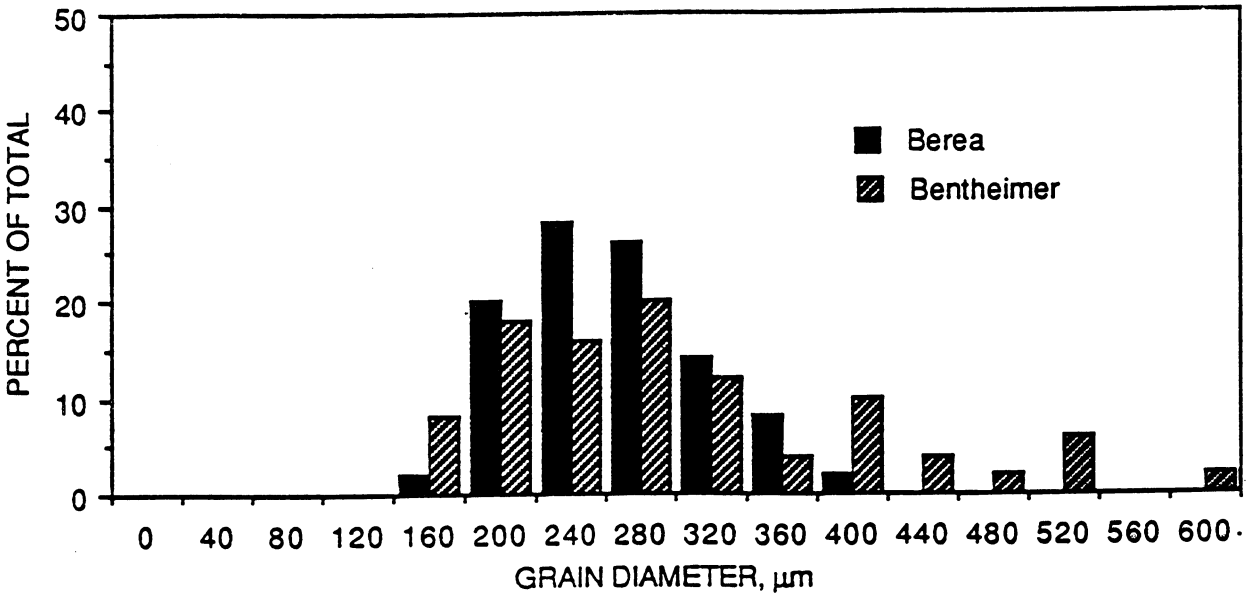

FIGURE 2A. - Grain diameter distributions by visual microscopic inspection.

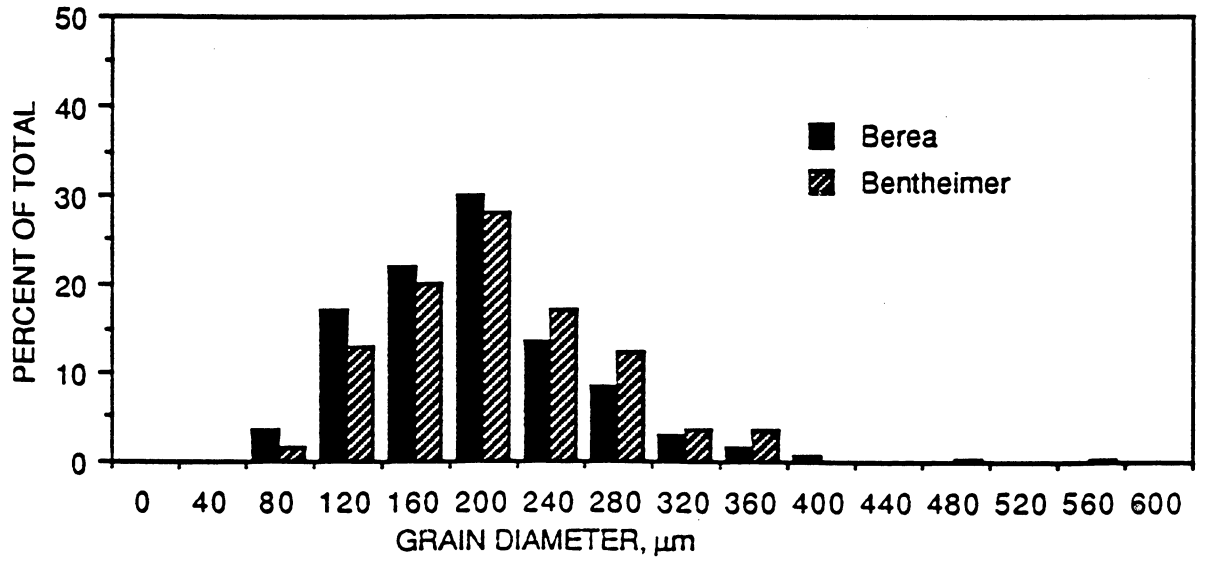

FIGURE 2B. - Grain diameter distributions by image analysis.

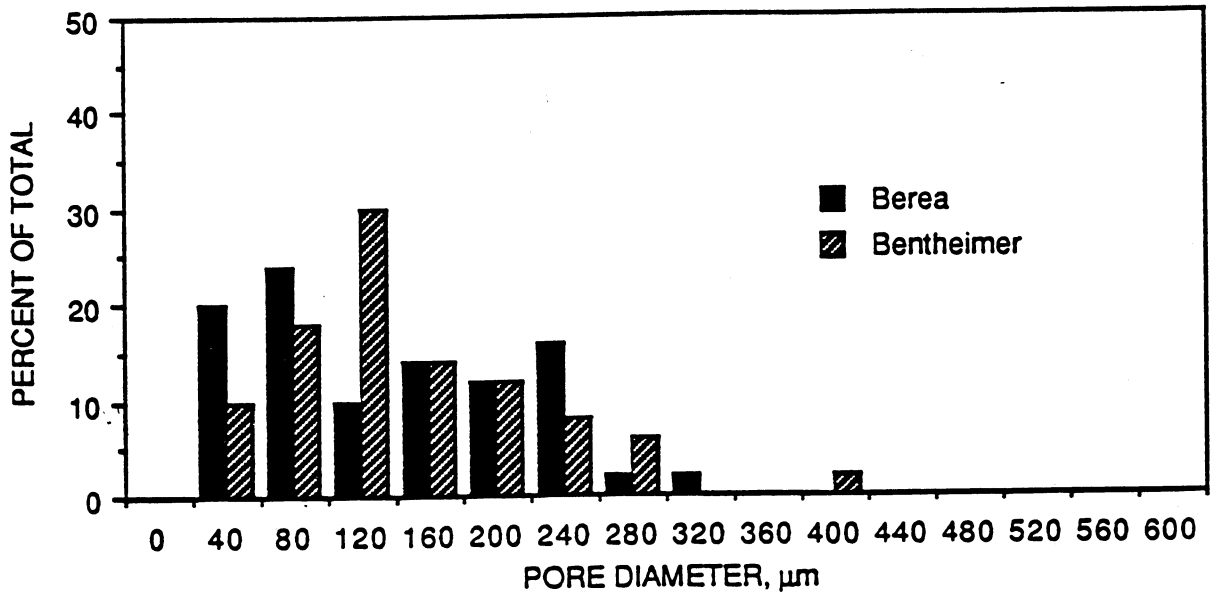

FIGURE 3A. - Pore body diameter by visual microscopic inspection.

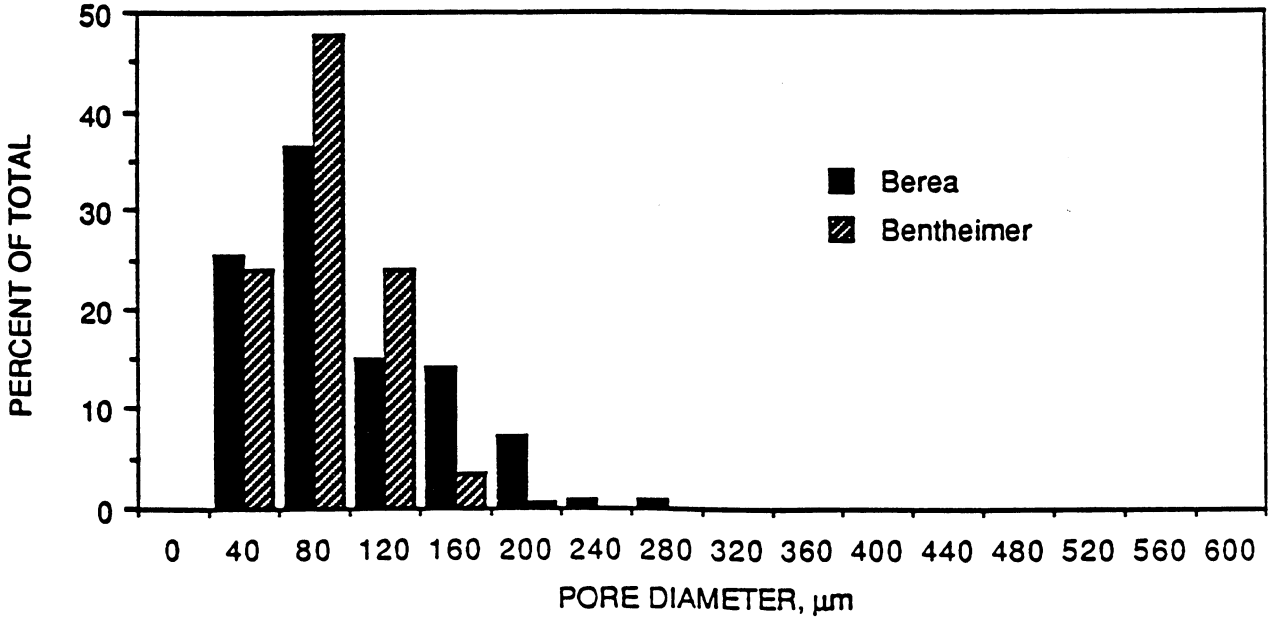

FIGURE 3B. - Pore body diameter by image analysis.

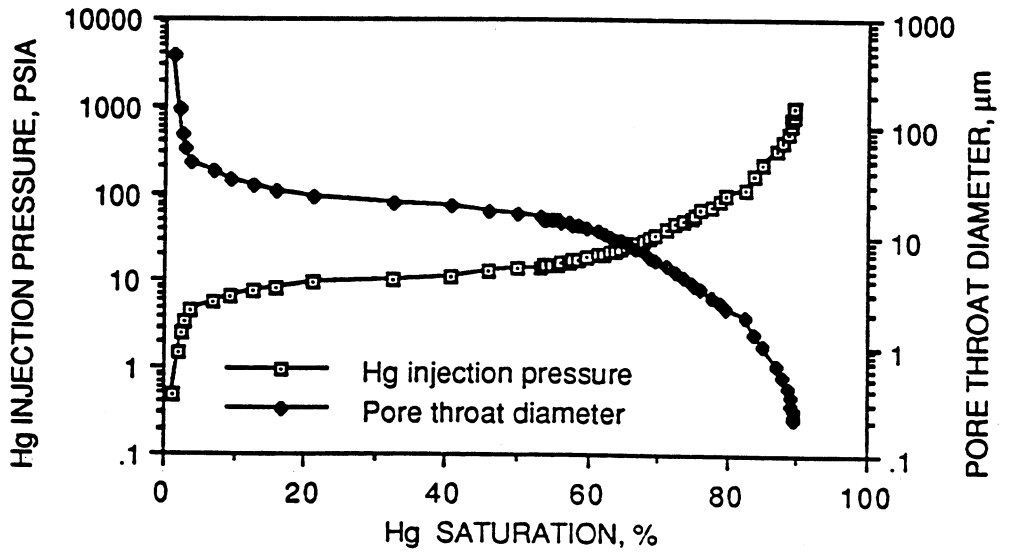

FIGURE 4A. - Mercury injection capillary pressure curves for Berea sandstone.

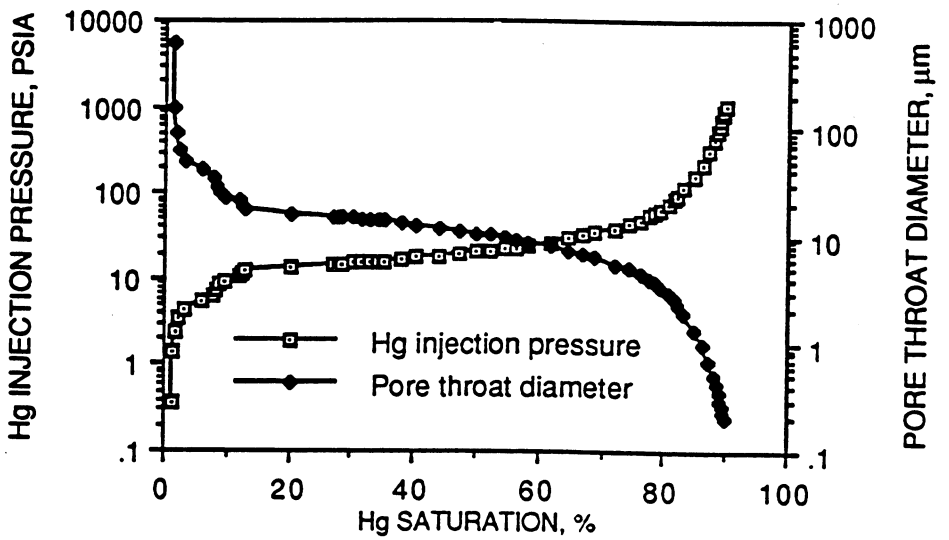

FIGURE 4B. - Mercury injection capillary pressure curves for Bentheimer sandstone.

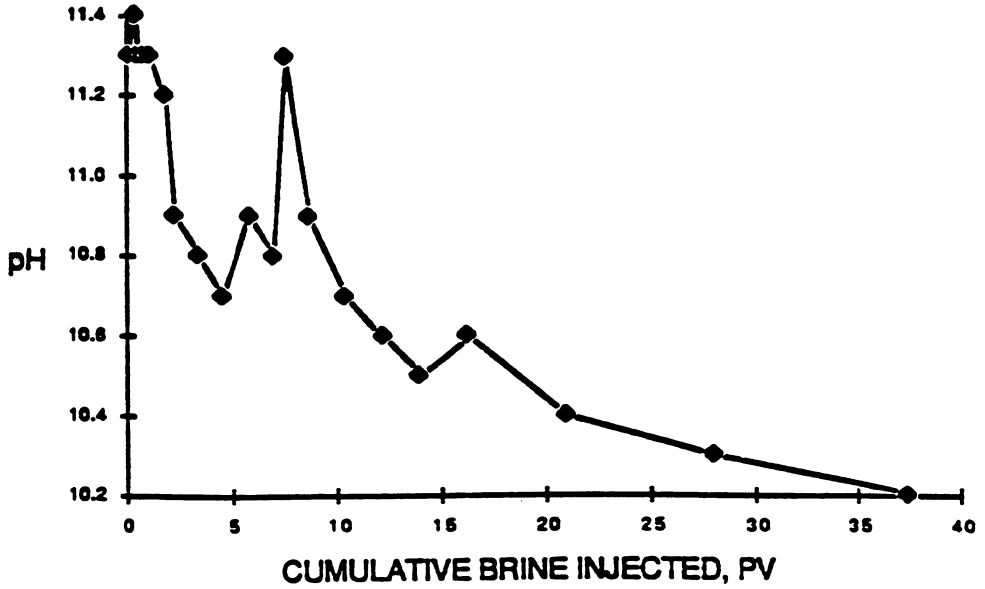

FIGURE 5. - pH of effluent brine measured during water permeability measurement test on fired Berea.

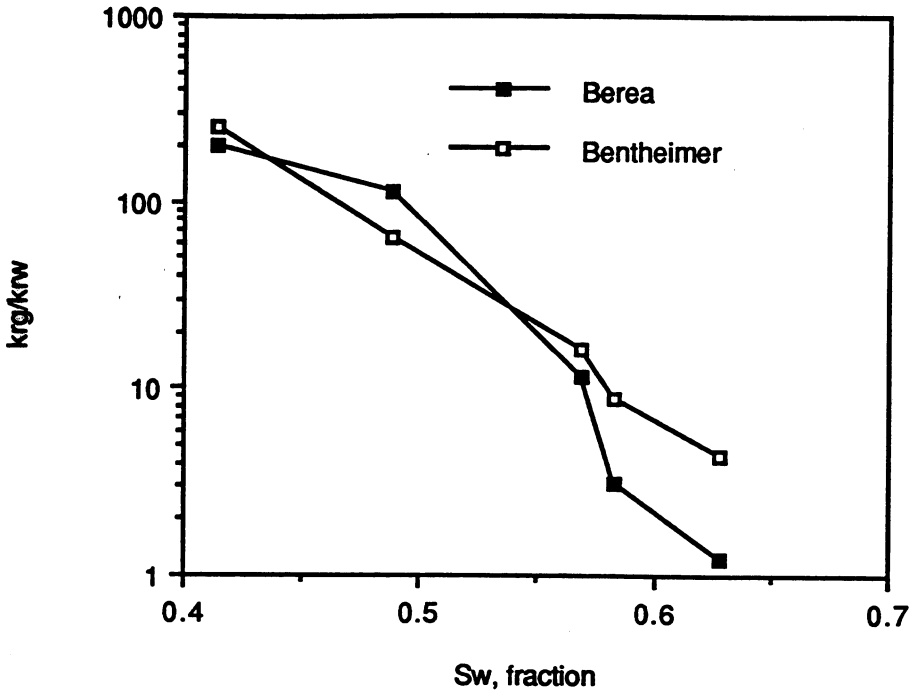

FIGURE 6. - Ratio of gas to water relative permeability plot for Berea and Bentheimer rock samples.

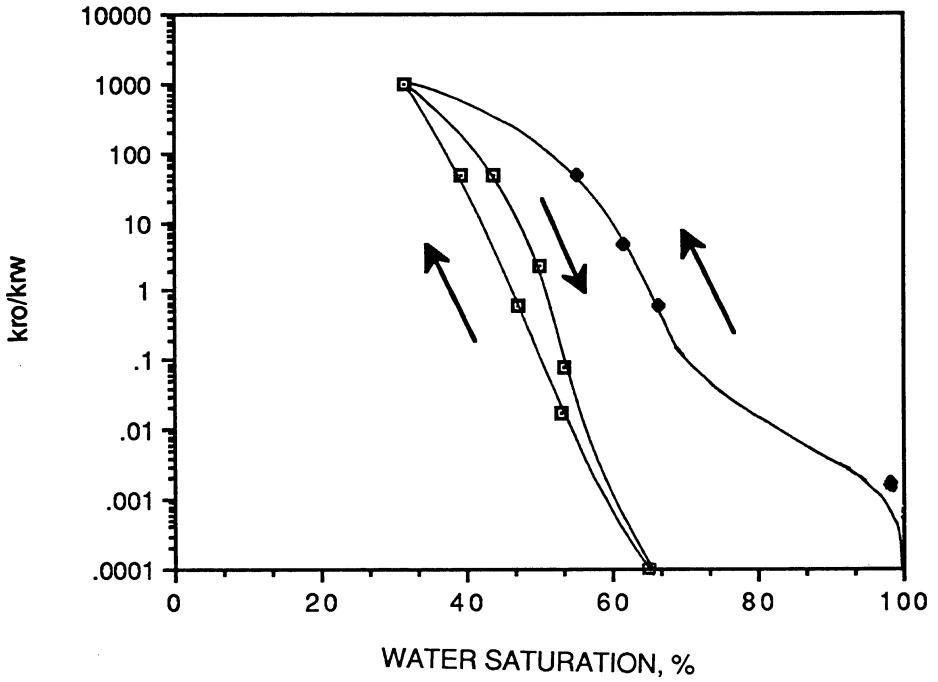

FIGURE 7. - Imbibition and drainage oil/water relative permeabilities for Berea sandstone.

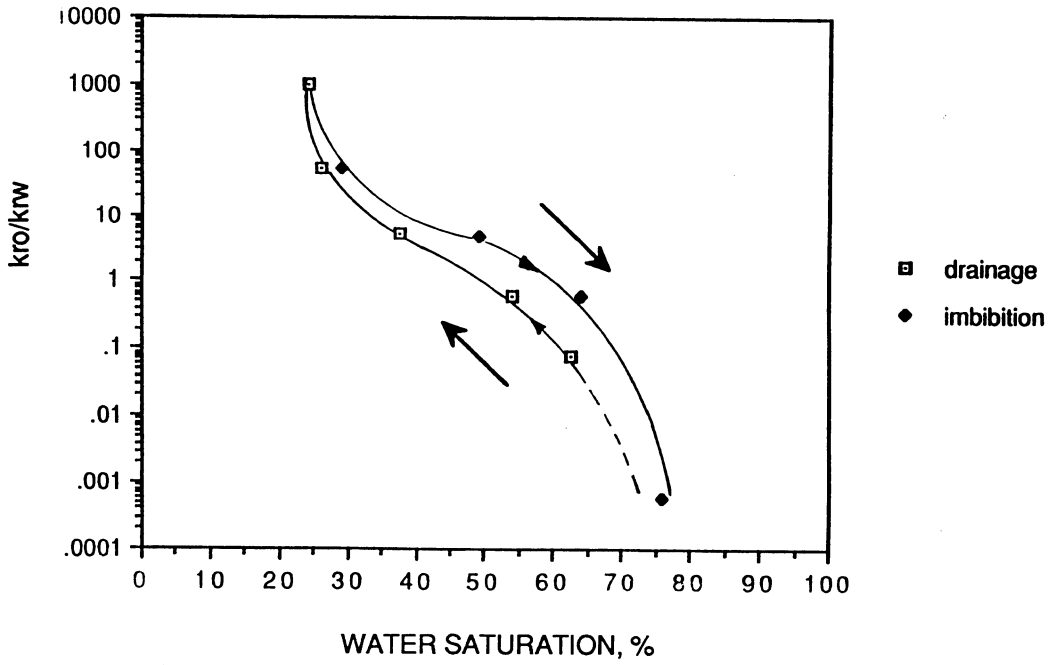

FIGURE 8. - Imbibition and drainage oil/water relative permeabilities for Bentheimer sandstone.

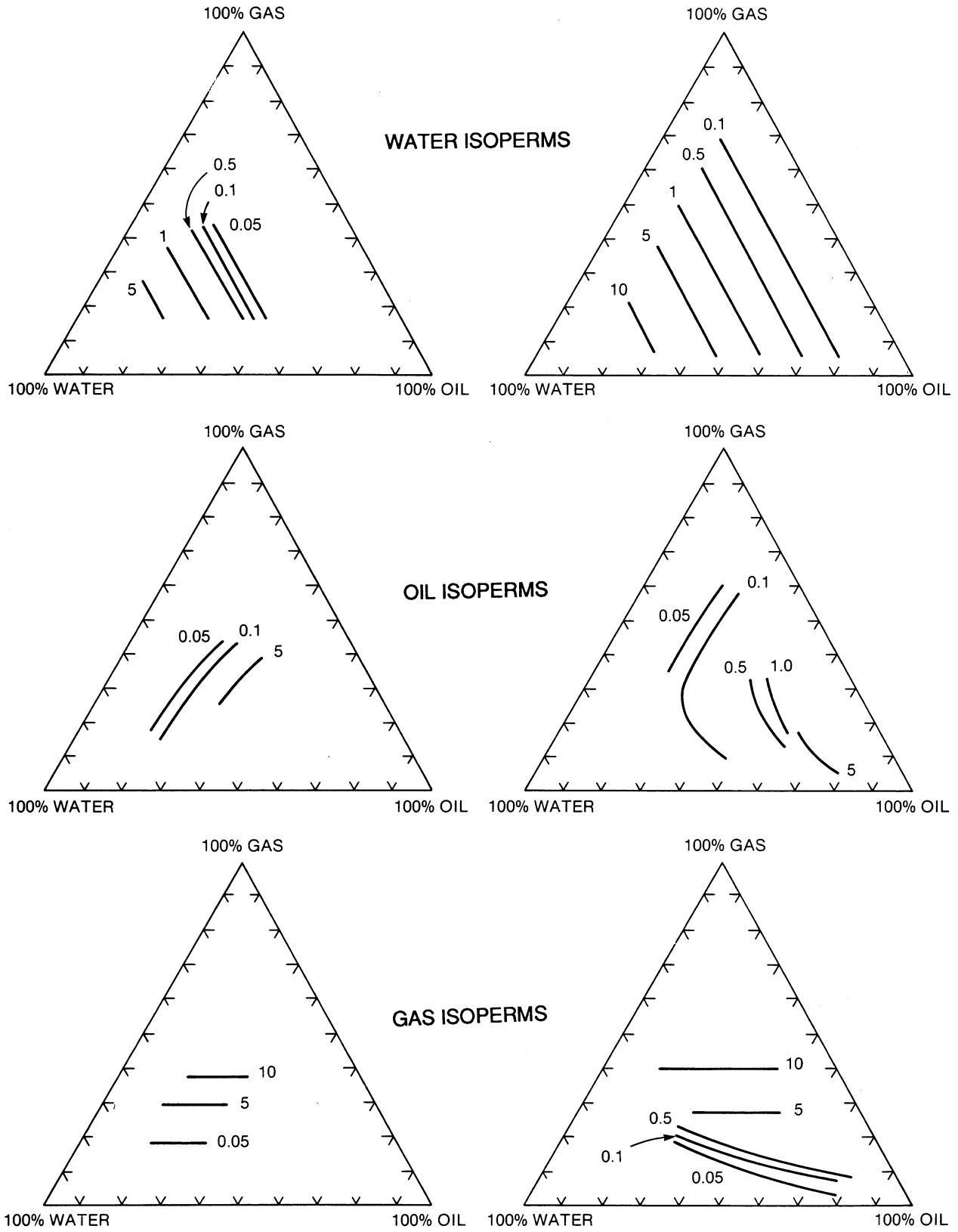

FIGURE 9. - Three-phase relative permeability results for Berea (left) and Bentheimer (right) sandstones. Isoperms shown are in percent.

APPENDIX A
X-RAY, MICROWAVE, AND PRESSURE MEASUREMENT SYSTEM IMPROVEMENTS

Microwave System

The microwave scanning system was improved by installing a high-sensitivity sensor to measure microwave power during core scans. Test results suggest that the scanning system is effective in characterizing brine saturations in cylindrical rock samples of 3.8 cm or larger diameter.

A sensitive K-band microwave power sensor with frequency coverage at the 21.3 GHz operating frequency of our microwave scanner was purchased. The sensor has measurement capabilities in the 100 to 10 microwatt range. The sensor was tested and found to be extremely sensitive to changes in water saturations within core plugs. Tests were conducted on a 3.8-cm-diameter core plug that was placed in a rubber sleeve within the composite material or microwave coreholder. The plug was subjected to 6.9 MPa confining pressure. X-ray and microwave scans were conducted as the plug was cycled through various oil and brine saturation conditions. Excellent X-ray response was attained using the cylindrical plug in the microwave coreholder.

Changes in X-ray attenuation were primarily due to changes in tagged-oil saturation. Sufficient microwave power emerged from the sample to allow measurement throughout the testing sequence, even when the plug was completely saturated with brine. The degree to which the microwave signal was attenuated under complete brine saturation conditions suggested that the microwave scanning equipment could be used for cylindrical samples of greater diameter than 3.8 cm. Test results indicated that even though mats of microwave absorbent were placed above and below the core, some of the microwave energy bypassed the core plug by taking a path above or below the core within the coreholder. Any gap between the cylindrical coreholder and the inner wall of the coreholder is a potential path for microwaves that do not pass through the rock to reach the power sensor on the emergent side of the coreholder.

It was evident from the results that further improvements in the microwave scanning system might be gained by designing better microwave absorbent fixtures to prevent microwave bypass or reflection. Two products, Eccosorb CR-S-117 and Eccosorb 269E, were purchased from Emerson and Cuming, Inc. The CR-S-117 is a high-loss, castable RTV silicone. The 269E is a high-loss epoxy formulation that can be brushed onto surfaces. The metallic surfaces of the microwave coreholder were painted with the 269E product to reduce the reflectivity of the

coreholder to microwaves. The CR-S-117 material was molded into bar-shaped fixtures that easily attach to the strengthening rods on the microwave coreholder. Both of these innovations should improve the characteristics of the microwave system.

Microwave scans of a heterogeneous glass micromodel were performed to examine whether the enhanced microwave scanner was sensitive enough to detect changes in brine saturation within the model. The model cross section was 0.023 by 6.2 cm, and the length was 8.4 cm. The increase in microwave power attenuation from a dry to a completely saturated state was 1.5 dB. Intermediate saturations were induced by injecting air into the model, yielding microwave power attenuation results which fell between the dry and saturated extremes. These results indicated that the microwave scanner may be well suited for quantifying average brine saturations in thin micromodels and for quantifying small changes in the brine content within porous media.

Additional materials were evaluated with the microwave scanning system in an effort to develop an inexpensive coreholder for permeability experiments in which samples are confined at pressures to 21 atm. PVC pipe, which is commonly used in construction projects, was found to have promise as a coreholder material. It is almost transparent to X-ray and microwave transmission. A prototype coreholder was fabricated using PVC pipe, but the design was discarded because the threads on the manufactured, glued-in collars would not hold pressure without leaking. Modifications were made to the end pieces to the coreholder, but leaks still prevailed. The PVC pipe didn't have a thick enough wall to allow threads to be cut directly into the PVC pipe. A coreholder barrel was then fabricated with a high-pressure, nylon material. The ends of the barrel were threaded to accept the end pieces. The nylon coreholder was also essentially transparent to microwave and X-ray transmission. Some leakage occurred around the o-ring seals on the end pieces. Because of this leakage, the coreholder was not used for experimentation this year. Additional work is required to machine end pieces that are leak-tight.

X-ray Data Utilization and Calibrations

The method used to calculate oil saturations during three-phase relative permeability tests was described previously[1] but was reported incorrectly. The correct mathematical expression for determining the oil saturation from both X-ray and microwave scan data is:

$$S_o = S_{o(o\text{-}w)} + \{S_{o(o\text{-}g)} - S_{o(o\text{-}w)}\}\{1 - S_w\} \quad \text{(A1)}$$

where

S_o = true oil sat.

$S_{o(o\text{-}w)}$ = oil sat. result from the oil-water X-ray correlation

$S_{o(o\text{-}g)}$ = oil sat. result from the oil-gas X-ray correlation

S_w = water saturation from the water microwave correlation

The difference between X-ray results (Ln(I)) for a rock under brine-saturated or oil- saturated conditions and the dry condition is proportional to the amount of the saturating liquid in the scan path. A means for determining the porosity distribution within a sample from X-ray scan data was developed. If the average porosity of the sample is known, then the porosity at each scan position can be calculated from:

$$\varnothing_i = \varnothing_{ave}\,[(Ln(I)_{dry} - Ln(I)_{sat.}]_i \,/\, [(Ln(I)_{dry} - Ln(I)_{sat}]_{ave} \quad \text{(A2)}$$

where $\varnothing_{ave}$ = average porosity of the rock

and subscript i denotes results at position i

This technique should be very useful for core samples in which the porosity and permeability vary greatly with length, or to evaluate the homogeneity of the rock sample.

Pressure Measurement Systems

The transducers used to measure both pressure drops and gauge pressures during relative permeability experiments were replaced with Rosemount differential pressure transmitters during the project year. The transmitters were selected due to their reputation for accuracy, long-term stability, and low maintenance requirements. The voltage drop across a precision resistor placed in the current loop for each transmitter is used as the measurement which is calibrated to pressure. The 4 to 20 mA output signal from one of the transmitters yields a 40 to 200 mV voltage signal that is read by the computer-automated data-acquisition system. The transmitters have performed well and have provided greater reliability to pressure measurements used for permeability calculations.

APPENDIX B
AUTOMATION OF THE LIQUID INJECTION SYSTEM

A three-pump system was constructed to allow continuous flow of two liquid phases (brine and oil) during the course of three-phase relative permeability measurements. This system uses two main Isco pumps (LC-5000) and a standby pump (LC-2600) for backup flow when either main pump is in the refill mode.This system resolves the shortcoming of pumps that have good accuracy but require the stoppage of flow for refilling during measurements of three-phase relative permeabilities. The cost of the construction of this system was approximately a third of that of the continuous system that is presently available on the market.

System components include 4 high-pressure, air-actuated, three-way fluid valves; two fluid transfer cylinders; and two refill reservoirs. The pumps and the three-way valves are operated by computer. A general schematic diagram of the system is presented in figure B-1. At startup, all pumps are full of liquid, and flow rates are set for the two main pumps. The three-way fluid valves 'B' and 'C' are set to direct flow from the main pumps to the core (see figure B-1). When either of the main pumps is in need of refill, as signaled by the computer program, the standby pump is activated, and the fluid is pressurized to the required injection pressure. Three-way valve 'B' or 'C' redirects flow to the core while one of the main pumps is refilled from the appropriate reservoir through either of the three-way valves 'A' or 'D'. The program commands the refill of the main pump and switches flow back to the main system when refilling is completed. This is accomplished by closing the 'A' or 'D' valve and opening the 'B' or 'C' valve.

The brine and oil reservoirs are pressurized with a cap of helium gas. The helium keeps air out of the brine and oil and aids in refilling the pumps. The helium cap pressure is 2 atm (abs). The reservoirs were fabricated from plexiglas so that the volume of liquid remaining in each reservoir is easily monitored.

The laboratory computer communicates with the pumps by means of an interconnection between the serial communication port of the computer and the serial interface of each pump. This interface allows programmable control using RS-232-C ASCII output. The programmed instructions allow control of all pump functions by computer (see figure B-2). The three-way valve system is controlled by the HP 3497, a data -acquisition/control unit using interface card 44431A, which is an eight-channel, high-voltage actuator. The actuator acts as a relay for switching a voltage to eight solenoid valves. Each solenoid valve controls one side of the pneumatic valve; therefore, eight solenoid valves are necessary to control the open/close status of all four three-

way valves. A detailed diagram for a single pneumatic valve automation is presented in figure B-3.

The automated pumping system was used for the Bentheimer sandstone flow tests. A software routine was added to the automation program to allow the operator to monitor pressure fluctuations graphically over an operator-selected time interval. This procedure gives the operator a means of determining whether a steady-state flow condition has been achieved. The pumping system and associated software performed well during the two-phase relative permeability tests and provided a simple criterion for switching to the next flow condition.

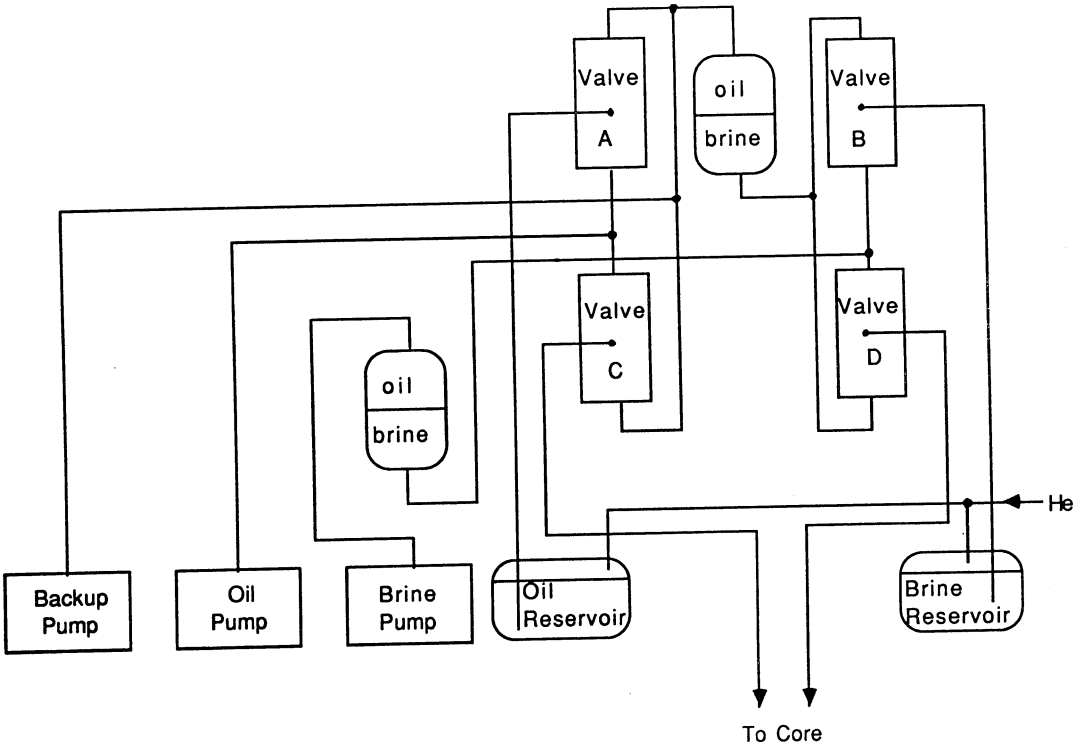

FIGURE B-1. - Schematic of pumping system for continuous injection of two liquid phases for relative permeability tests.

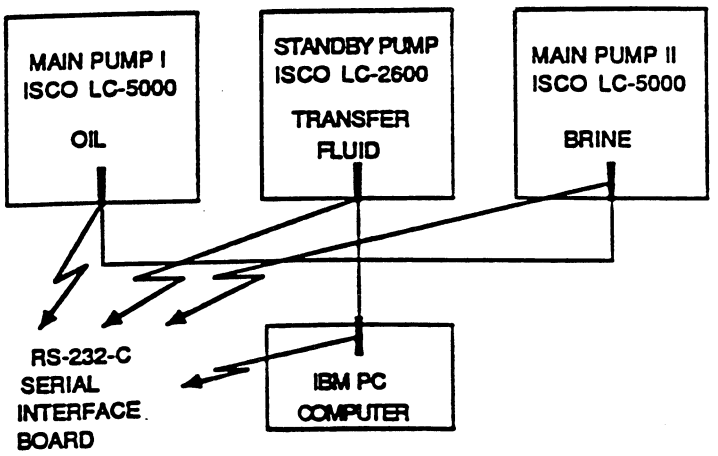

FIGURE B-2. - Computer-pumps communication system.

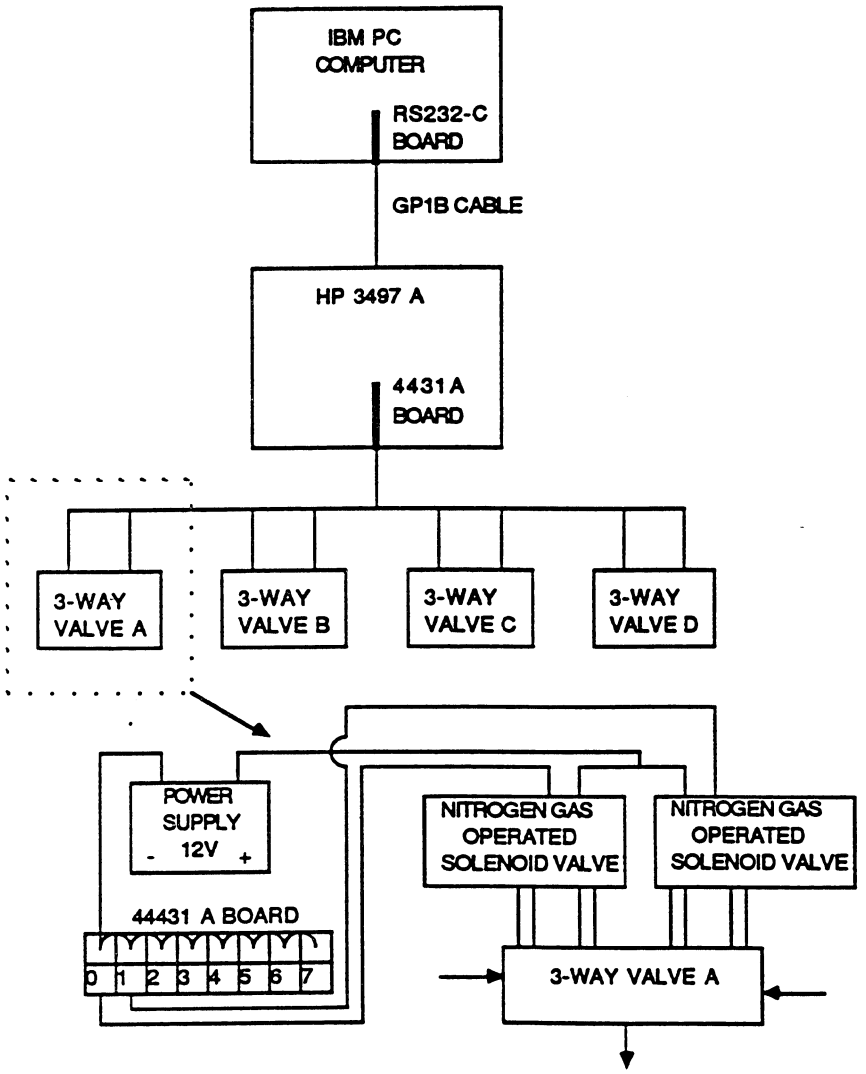

FIGURE B-3. - Detailed diagram of single pneumatic valve automation.

☆U.S. GOVERNMENT PRINTING OFFICE: 1990- 761-030/00067